Strain Inhomogeneities in Highly Oriented Gel-Spun Polyethylene

T. Amornsakchai,† A. P. Unwin, I. M. Ward,* and D. N. Batchelder

Department of Physics, University of Leeds, Leeds LS2 9JT, U.K.

Received October 1, 1996; Revised Manuscript Received May 19, 1997[⊗]

ABSTRACT: The nature of the stress/strain distribution in a highly oriented gel-spun polyethylene under stress has been examined using several techniques. X-ray diffraction has been used to characterize the crystalline strain; these results are compared with the macroscopic stress and strain and with the frequency of the 1060 cm^{-1} Raman band. It is shown that the Raman measurements effectively monitor the response of the crystallites and that any sensitivity to taut tie molecules is only a possible consideration at very high stress. A modified fiber composite model is considered the most suitable for predicting the mechanical behavior. It is also suggested that the reinforcement is provided by the microfibrils, which have the required large aspect ratio. At low applied stress, the buildup of stress along the fibril is very rapid, and consequently there is little evidence of stress/strain inhomogeneity. At high stress, however, strain inhomogeneities, which are dependent on temperature and time, are detectable in the crystalline regions. This behavior is also interpreted using a fiber composite model, and the implications for the stress buildup along the fiber are discussed.

Introduction

The relation between applied macroscopic deformation and the consequent molecular or microstructural response is of fundamental importance to an understanding of the mechanical properties of polymeric systems. The crystalline response can be monitored precisely using wide-angle X-ray scattering (WAXS), because the shift in 2θ space of a diffraction profile relates directly to crystalline strain parallel to the scattering vector. In principle, the molecular response can be examined using the frequency shifts of appropriate vibrational modes in infrared or Raman spectroscopies.[1,2] Interest in the latter has developed considerably in recent years as improvements in efficiency and spatial resolution, essential for examining microstructural behavior, have become available. The interpretation of Raman spectroscopic measurements, however, is complicated for several reasons. First, whereas WAXS is structurally specific, Raman spectroscopy tends to be conformationally specific, so that information obtained relates to both crystalline regions and taut tie molecules. Even so, this can be advantageous if the different sets of information can be decoupled. A more serious difficulty concerns the physical origins of the peak shifts.

Early studies[3,4] on Raman peak shifts in a deformed single crystal fiber embedded in a matrix showed a linear relation between peak shift and the strain measured in the direction of the applied force. The crystal strain was generated by deforming the matrix in which the crystal was embedded, and the behavior was found to be relatively consistent with a Cox model analysis. The simple relation between stress and strain in such systems renders it difficult to conclude whether it is the stress or the strain that is responsible for the peak shifts. Recent work by Lewis et al.[5] on poly(ethylene terephthalate) has shown that the peak shift is not simply related to either the stress or the strain in less highly aligned systems. Clearly then, there is some uncertainty concerning the interpretation of Raman peak shifts. Nevertheless the technique does provide a deeper insight into the structural nature of materials, especially when complemented by measurements from other techniques.

Generally, the application of small stresses or strains to oriented samples of polyethylene produces a positional shift but leaves the shapes of both spectroscopic and X-ray diffraction profiles relatively unaffected. In highly drawn gel-spun polyethylene, particularly at high stress, however, the positional shift is accompanied by the development of pronounced asymmetry, and in some circumstances the splitting, of the peak profile. Tashiro et al.[6] observed this effect using Raman spectroscopy, and explained the peak splitting in terms of stress/strain inhomogeneities at the molecular level. These results prompted a greater interest[7−10] in the phenomenon because it offered the prospect of explaining the observation that experimental strengths are considerably less than theoretical estimates. More recently, changes in the peak shape have also been observed in X-ray diffraction.[11,12] The simplest interpretation of both the Raman and X-ray peak splitting assumes a bimodal stress/strain distribution and different structural models following Takayanagi[13] have been proposed.[6,9,14] A more complex analysis involving distributions of stress/strain that accompany a fiber composite approach has also been undertaken.[15]

The investigation of the structural nature of a material benefits not only from the use of complementary techniques but also from an investigation of the temperature dependence of the different responses. Such an approach is useful because it offers a simple means of altering the stress transfer between structural units within the material, providing an independent means of assessing structural alternatives. Here, we combine measurements derived from X-ray scattering and simple mechanical tests, conducted at different temperatures, to identify a suitable structural model for highly drawn gel-spun polyethylene. The results from Raman microscopy are then examined in the light of these conclusions.

* To whom correspondence should be addressed.
† Present address: Department of Chemistry, Mahidol University, Rama 6 Road, Bangkok 10400, Thailand.
⊗ Abstract published in *Advance ACS Abstracts,* July 15, 1997.

S0024-9297(96)01462-3 CCC: $14.00

Table 1. Properties of *Spectra 1000* (Taken from Ref 16)

property	value
modulus/GPa	172
ultimate tensile strength/GPa	3.09
elongation/%	2.7
tex/g km^{-1} (denier)	72 (650)
filament/yarn	120
filament diameter/μm	27
density/g cm^{-3}	0.97

Experimental Section

Material. A high modulus commercially available gel-spun polyethylene fiber *Spectra 1000* manufactured by Allied-Signal was investigated in this work. The properties of the material (a yarn with 120 filaments) are shown in Table 1.[16] The melting behavior, at a heating rate of 10 K min^{-1}, was examined using a Perkin Elmer differential scanning calorimeter (DSC7). A crystallinity value of 80% was obtained from the area of the melting endotherm.

A major problem with this material concerns the uncertainty in the cross-sectional area of the filaments. Individual measurements of filament diameter, made using a microscope, produced a mean diameter of 35 μm with a standard deviation of 5 μm. This is considerably different from the quoted value of 27 μm probably because the filaments do not have a circular cross section and the technique of viewing under a cover slip tends to pick up the major axis dimension. The value of 27 μm is consistent with measurements of mass per unit length of the yarn and the sample density and hence is considered the more reliable mean. Where troublesome, the problem of the large standard deviation in the diameter is overcome by combining appropriate key measurements on a single filament with repeated simple measurements on different filaments.

Isochronal Creep Modulus. The 20 s isochronal extensional creep modulus was measured at several temperatures on single filaments extracted from the yarn. Measurements were performed on the same specimen so that variations in the cross-sectional area, inevitable in these highly irregular filaments, did not contribute to measured differences in mechanical properties occurring with temperature. Before measurement, all samples were subjected to a five cycle conditioning procedure. Each cycle consists of a loading stage, using a load slightly greater than any in the subsequent experimental procedure, followed by a recovery stage. The loading time, chosen to correspond to the minimum value suitable for X-ray diffraction experiments, was 20 s and the recovery time 10 times this value, namely 200 s.

The extension of the sample after 20 s was recorded as a function of applied load using apparatus and procedure outlined elsewhere.[17] The extension is defined as the difference between the unloaded transducer reading and that after loading for 20 s. The unloaded reading was taken to be the average of readings before loading and after recovery except where nonrecoverable creep was a problem, in which case the reading before loading was used as the reference. This was only necessary for measurements at high temperatures.

X-ray Diffraction. A length of yarn (multifilament ~25 mm long) was mounted in special clamps in a manner designed to ensure as equal a stress distribution between filaments as possible, and the clamps attached to an extensometer. The extensometer was specially designed to ensure that lateral movement of the sample during loading was very small (<20 μm); otherwise, measurements of peak shift, from which the crystal strain is calculated, could include a significant contribution from sample translation. The whole system was placed at the center of a Philips diffractometer table with the sample in transmission mode so that the (002) reflection appeared on the position sensitive detector, details of which can be found elsewhere.[18] The sample orientation was optimized to ensure maximum diffracted intensity. A conditioning procedure, described above, with loading and recovery times of 20 and 200 s respectively was performed and subsequently scattered intensity profiles were recorded as a function of loading. Measurements were carried out at −55 °C, room temperature and 50 °C using copper Kα radiation.

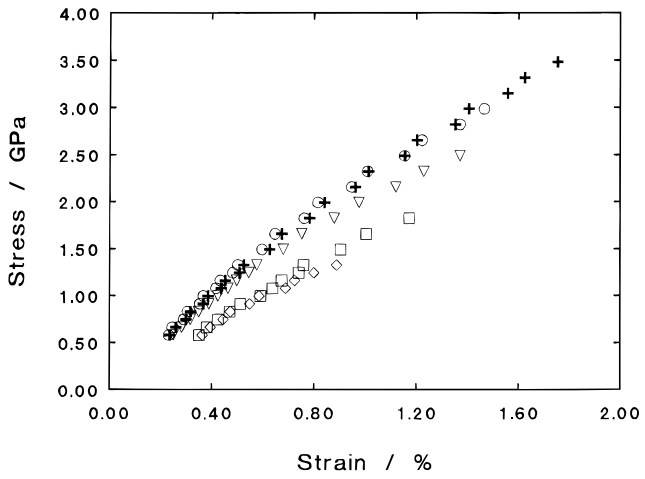

Figure 1. 20 s isochronal stress−strain curves for a single filament of *Spectra* at 50 °C, ◇; 21 °C, □; 0 °C, ▽; −30 °C, ○; and −55 °C, +.

Raman Spectroscopy. Raman spectra with a spectral resolution of ~2 cm^{-1} were obtained on a Renishaw Raman microscope using the 633 nm line of a relatively low power (~8 mW at the sample) He−Ne laser for excitation. An Olympus microscope equipped with a ×20 objective (NA 0.4) was used to focus the incident beam and collect the Raman-scattered light. The laser spot diameter on the fiber was about 4 μm. Unpolarized spectra were recorded in backscattering geometry for the incident beam polarized perpendicular to the fiber axis. The 1060 cm^{-1} band, which is stronger under these circumstances, was therefore used to monitor the C−C bond deformation. This contrasts with other work where the incident polarization is parallel to the fiber axis and analysis is concentrated on the 1125 cm^{-1} band.[8,9,11] Some limited measurements were performed for polarization parallel to the fiber axis using the 514.5 nm line from an argon ion laser to check sensitivity to wavelength and polarization.

Spectra were obtained from single filaments during deformation in a small stretching rig that fitted directly onto the microscope stage. The fiber was strained in a dead-load creep type of experiment. A gauge length of 25 mm was used. Again a conditioning procedure using loading and recovery times of 20 and 200 s, respectively was performed before measurements were recorded. Investigations were carried out at room temperature and at −55 °C in a small rigid polyurethane foam enclosure with a glass window.

Results

Isochronal Creep Modulus. Figure 1 displays 20 s isochronal stress−strain curves for a single filament at different temperatures. These results derive from the same specimen, so the relative behavior with temperature is not subject to errors introduced by variations in cross-sectional area between filaments. The error in the absolute value for the stress arising from this variance has been minimized by scaling the stress appropriately to produce the same room temperature modulus with this filament as was obtained by averaging results obtained on five different filaments (equivalent to assuming a mean diameter for this filament of 27.4 μm). Data in the low stress region could not be obtained directly because of the finite load (30 g) of the transducer lug carrier. Essentially, the curves are linear at low temperature and strain, although a slight curvature is noticeable at higher strains.

The 20 s secant modulus at different levels of strain is plotted as a function of temperature in Figure 2. The error in the modulus is estimated to include a 4% uncertainty derived from the results of measurements

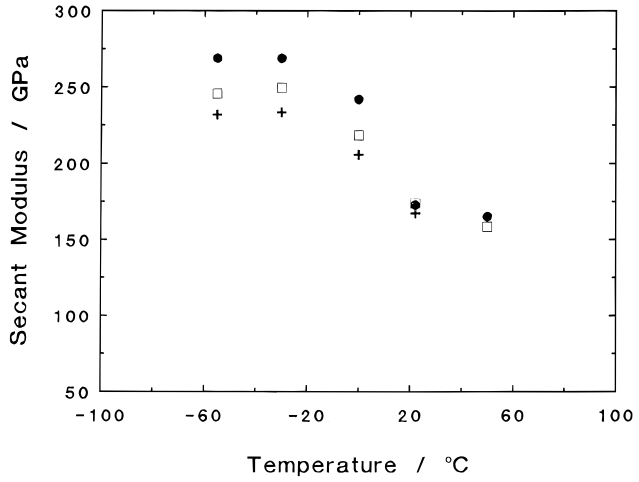

Figure 2. 20 s secant modulus at strain $e = 0.4\%$, ●; 0.8%, □; and 1.0%, +, as a function of temperature.

on 5 different filaments. The room temperature modulus agrees well with that quoted by the manufacturers (Table 1). Clearly the modulus decreases as either the strain or temperature are increased.

X-ray Diffraction. Figure 3 shows typical (002) diffraction profiles obtained at three temperatures (−55 °C, 21 °C and 50 °C) for different levels of applied stress. For convenience the graphs display the intensity as a function of channel number instead of 2θ, but there is a direct relationship between these two. Generally, as the stress increases, the (002) diffraction peak shifts to lower 2θ and develops an asymmetry, particularly pronounced at high stress, where the profile seems composed of two separate peaks. The nature of the asymmetry and the relative components of each peak depend on temperature.

The shift in peak position relates directly to the change in separation of the (002) planes in crystals that have their *c*-axes parallel to the scattering vector and, hence, because of the experimental alignment, parallel to the direction of the applied stress. (Strictly speaking, a genuine 2θ scan is necessary for this condition to be exact.) Two ways of analyzing the data are considered here. First, the observed behavior is considered to be the sum of the response from two separate populations of crystals, and the Bragg equation is used to find the *c*-axis strain for each population. This approach was prompted by the obvious splitting into two component peaks at very high stress. The individual peak positions are identified by curve fitting two Gaussians to the (002) diffraction profile. The second approach uses a template method to find the *average* crystal strain and has the advantage of removing a large element of the uncertainty arising from the first method. Results obtained from working directly on the observed data using the template method, found to be very successful when examining asymmetric peaks in liquid crystal copolymers,[18] are in agreement with those obtained by averaging the peak positions derived from curve fitting, taking account of the relative proportions of each peak.

The crystal strain at different temperatures, obtained assuming two distinct crystal populations, is plotted as a function of applied stress in Figure 4. In general, the crystalline phase responds similarly to stress at all temperatures. In the low stress region there is little, if any, distinction between the two populations and for both, the crystal strain increases linearly with stress. At high stress, however, the distinction between the two

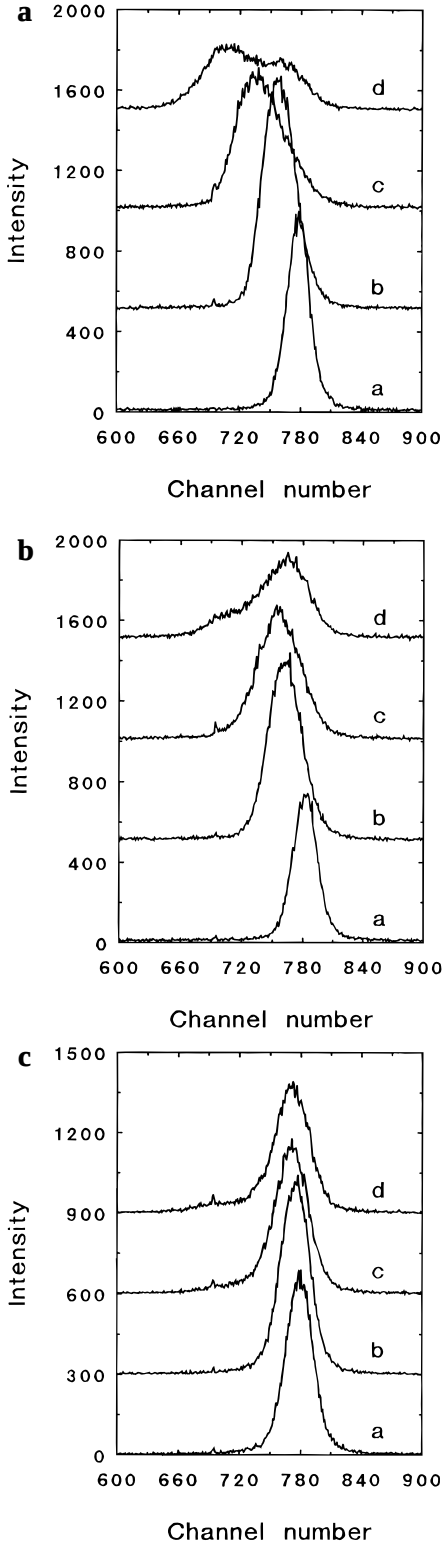

Figure 3. (002) diffraction profile of *Spectra* fiber subjected to different stresses at (a) −55 °C, (a) 0.2 GPa, (b) 1.4 GPa, (c) 2.46 GPa, and (d) 3.39 GPa; (b) 21 °C, (a) 0.2 GPa, (b) 1.4 GPa, (c) 1.93 GPa, and (d) 2.46 GPa; and (c) +50 °C, (a) 0.46 GPa, (b) 0.73 GPa, (c) 1.4 GPa, and (d) 1.66 GPa.

populations is obvious. Strain in one group increases sharply with increasing stress while strain in the other drops slightly. The differences seen with temperature concern the stress at which the separation occurs and the relative division of strain between the two populations. This second point is not noticeable from Figure 4 but can be appreciated from Figure 3. The balance between the high and low load bearing components is,

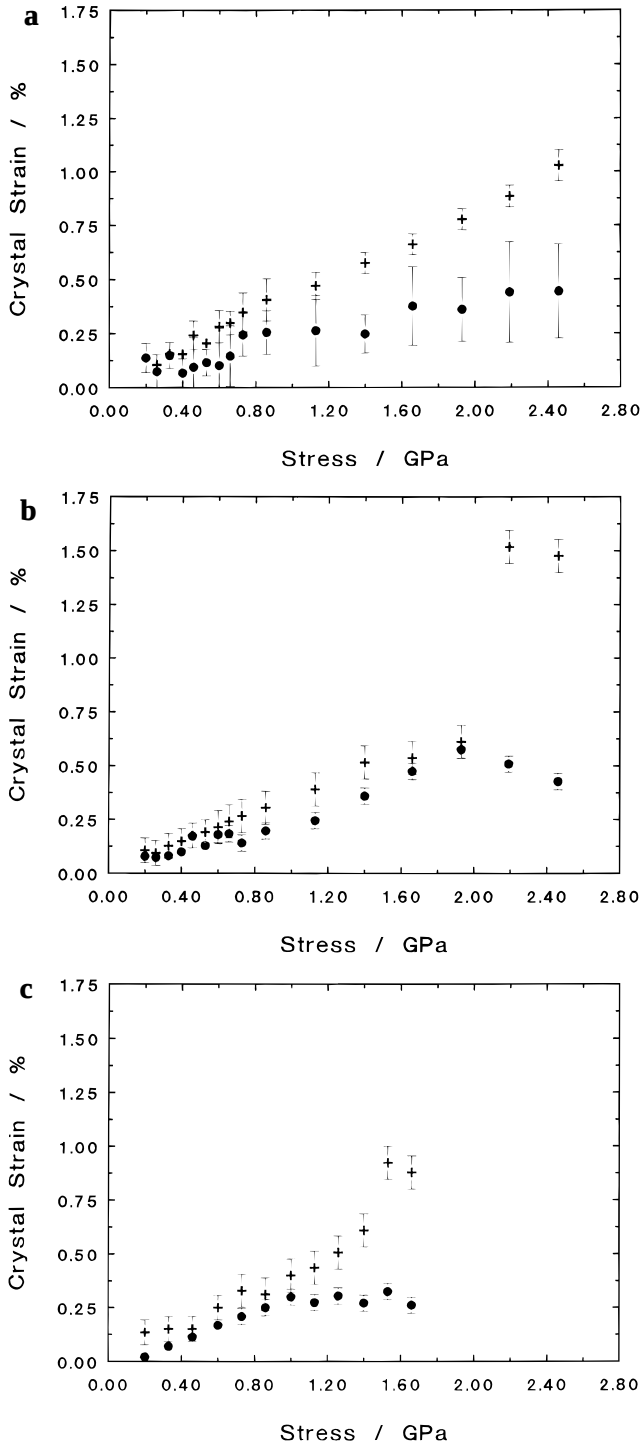

Figure 4. Crystal strain as a function of macroscopic stress, assuming two separate crystal populations: +, high load bearing, and ●, low load bearing at (a) −55 °C, (b) room temperature, 21 °C, and (c) 50 °C.

respectively, approximately 75%:25% at −55 °C, 25%:75% at 21 °C, and 20%:80% at 50 °C.

In these experiments the load applied to the sample during the loading cycle was systematically increased in steps up to the maximum value. The loading profile then followed a decreasing path at intermediate values so that any structural changes or stress strain hysteresis could be identified from differences in the two responses. In addition, a second series of measurements at −55 and 21 °C was performed on the same sample after the first series had been completed. The good correspondence between the different stages of the loading experiment and the different data sets showed that there was no significant hysteresis in the stress strain behavior and that structural changes occurring during loading could be neglected. This applies up to a stress of 2.46 GPa but may not be the case at very high stresses. Information relating to the highest stress, 3.39 GPa at −55 °C (Figure 3a), where a clear double peak is seen in the spectrum, was only obtained as the sample was taken to failure.

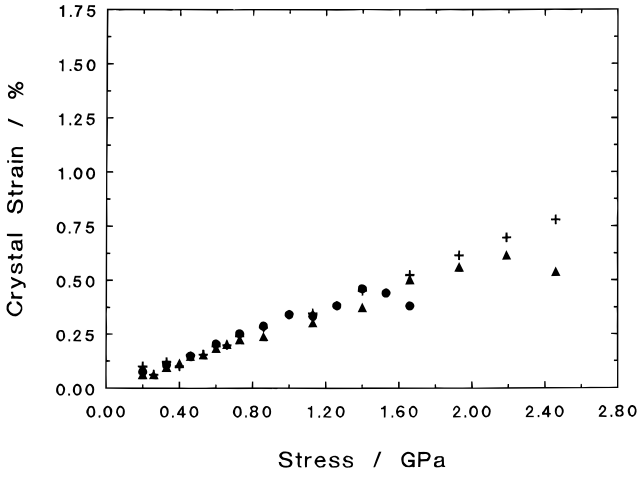

Figure 5. Average crystal strain as a function of stress at −55 °C, +; 21 °C, ▲; and 50 °C, ●.

The results of interpreting the X-ray data in terms of the average crystal strain are shown in Figure 5. Surprisingly, the response of the average crystal strain to stress is similar at all three temperatures. All show a basically linear response up to a critical stress. At −55 °C this linearity continues up to about 2.4 GPa but at room temperature and 50 °C a difference in behavior is detected at lower stress, namely, 2 and 1.4 GPa respectively. At stresses higher than these critical values the average crystal strain drops slightly. The implication is that above this critical stress the crystallites no longer experience additional load and there is a redistribution of stress away from the crystalline regions as a whole, presumably to the noncrystalline regions. This occurs, however, at stresses above which there is already an inhomogeneous stress distribution within the crystalline phase, as is evidenced in the asymmetry of the (002) profile.

This "saturation" of crystal strain at high stress has also been noticed in conventionally produced polyethylene[1] (draw ratio of five) as well as in single filaments of *Spectra* fiber by Prasad and Grubb,[7,19] who termed the point at which the crystal strain starts levelling off a "break point". By studying different grades of *Spectra* fiber, they found that this "break point" related to the breaking stress of the fiber with stronger fibers showing a higher "break point". Their results, however, did not show any sign of nonuniform strain at high stress. Moonen et al.[11] recently studied an experimental gel-spun/hot-drawn polyethylene fiber, *Dyneema*, and found that at high stress the crystal strain saturates. Furthermore, at high stress, this material also showed nonuniform crystalline strain.

It is important to be aware of a fundamental limitation of the experimental technique considered here, arising from the directional dependence of the scattering vector on 2θ and the limited divergence of the X-ray beam. The range of scattering vectors sampled depends on the beam divergence, so that, ideally, as the crystals

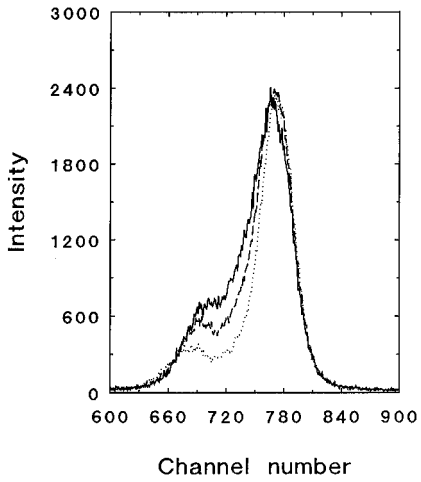

Figure 6. Time dependent behavior of the (002) diffraction profile for a stress of 2.46 GPa at room temperature (21 °C). 5 sec, (—); 20 sec, (- - -); and 100 s, (···).

Table 2. Positions and Area Fractions of (002) Composite Peaks for Different Loading Times at Room Temperature[a]

loading time/s	position of peak A (2θ)/deg	position of peak B (2θ)/deg	area fraction of peak A/%
5	73.12	74.06	36
20	73.00	74.09	31
100	72.87	74.13	26

[a] Stress is 2.46 GPa. Peak A is the high load-bearing component.

are strained (and 2θ changes), the sample needs to be rotated to ensure the detector still samples the appropriate crystals. This is the procedure in a genuine 2θ scan. When the sample is not rotated, however, the scattering vectors related to crystallites showing large changes in 2θ move outside the sampling range of the detector. Therefore, the technique is ineffective at monitoring highly strained crystals, oriented along the direction of applied stress; i.e., very high strain information is lost. For the data presented here the integrated intensity in 2θ space only starts to fall at very high stresses where the curves in Figure 5 deviate from linear so that the strain saturation may be a reflection of the limitation of this technique.

The apparent crystal modulus, derived from the low strain behavior in Figure 5 and assuming that the crystalline stress is identical to the macroscopic stress, (homogeneous stress) is 290 GPa. This is in line with the value reported by Prasad and Grubb[7,19] for a single fiber of *Spectra* at room temperature but differs from measurements on conventionally produced material.

Finally it is important to note that the X-ray response to stress is time dependent, certainly at high stress. Figure 6 shows the (002) diffraction profiles collected from a sample subjected to a stress of 2.46 GPa at room temperature for different loading times. It was necessary to sum multiple exposures for the short time experiments. The curves have been normalized to give the same maximum intensity for one of the peaks. The results of free fitting to these profiles are shown in Table 2. Clearly, as the loading time increases the relative area of the smaller, high load-bearing peak decreases while its position shifts slightly towards lower 2θ. This time dependent response shows the importance of using a fixed loading time for all experiments.

Raman Spectroscopy. Preliminary work on samples subjected to loading showed that in the spectral range, 1000−1500 cm^{-1}, both the positions and the shapes of

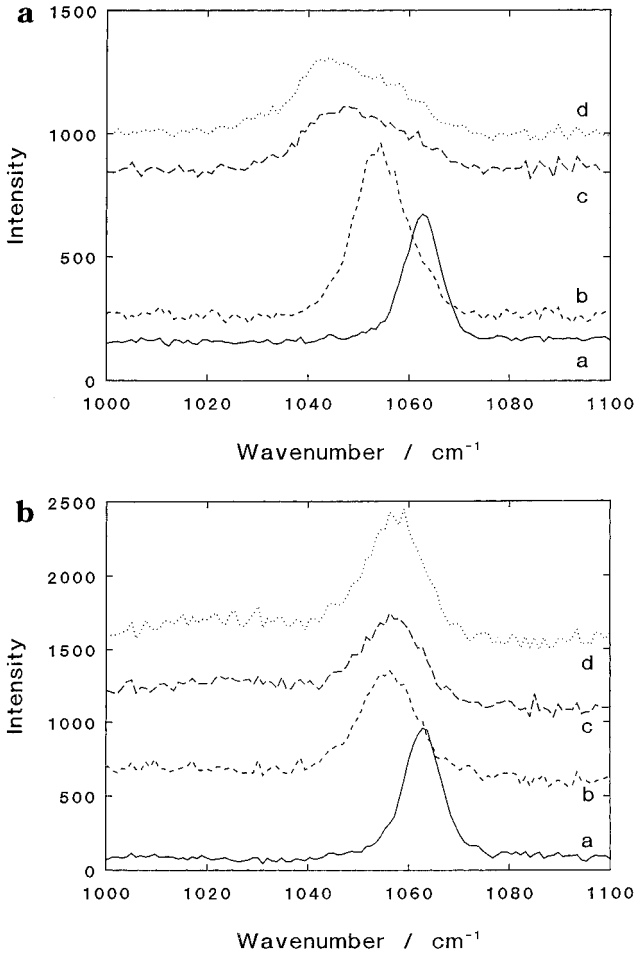

Figure 7. Raman spectra of polyethylene fiber subjected to different stresses at (a) −55 °C and (b) 21 °C. Stress levels in each part (a) 0 GPa, (b) 1.2 GPa, (c) 2.25 GPa, and (d) 2.4 GPa.

many bands are sensitive to stress. Here, interest is concentrated on the 1060 cm^{-1} and, to a lesser extent, 1125 cm^{-1} bands, both associated with C−C bond vibrations. Parts a and b of Figure 7 show the behavior of the spectrum around the 1060 cm^{-1} band in a sample subjected to different stress levels at −55 and 21 °C respectively. At these temperatures the 1060 cm^{-1} band shifts to lower frequencies and becomes broader as the stress is increased. This shift to lower wavenumber with increasing stress has been reported by other researchers[2,6,7,9] and is generally attributed to bond anharmonicity;[2,20,21] i.e. the force constant decreases with increasing strain. It is also apparent that as the stress increases, a pronounced asymmetry develops. At 21 °C the very high stress profiles can be resolved into two composite bands, with that at low wavenumber being very broad. Band splitting in stressed polyethylene has been seen previously in *Spectra*[7] and also in an experimental gel-spun/hot drawn fiber (*Dyneema*).[8,9,11]

Figure 7 also shows that as the applied stress is increased, the intensity of the Raman scattered light initially increases before subsequently decreasing. The initial rise is possibly due to a small improvement in the orientation as kinks are removed. The drop in band intensity at higher stresses probably relates to an increase in scattering from microvoids. The presence of microvoids in drawn polyethylene is well-known and often leads to sample whitening in very highly drawn material. In addition, the penetration of the laser beam depends on the clarity of the material, and a reduced

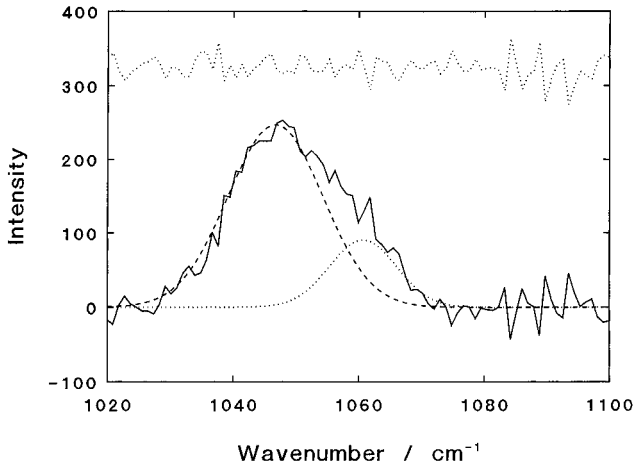

Figure 8. Example of a 2 Gaussian component fit to curve c in Figure 7a (2.25 GPa at −55 °C). The difference spectrum is shown displaced above the experimental and fitted data.

penetration arising from a high microvoid concentration may result in the Raman data being more representative of the fiber skin.

A detailed breakdown of the behavior of the two components of the 1060 cm^{-1} band was obtained by curve fitting using two Gaussian line shapes; this provided a much better fit to the Raman spectra than two Lorentzians Although Lorentzian line shapes generally provide better fits to spectroscopic data, any effect that produces a statistical averaging of the signal, such as stress distributions, can lead to a smearing of the intrinsic line shape resulting in a more Gaussian profile. Figure 8 shows an example of such fitting to curve c in Figure 7a. The difference spectrum shows that the fit is quite good and provides confidence in this approach to identifying the component bands.

Figure 9 shows the positional shift of these component bands with stress at two temperatures, −55 and 21 °C. Again, as was the case for the X-ray measurements, the nature of the loading program and the repeated measurements on the sample confirm that there is no significant hysteresis or structural change up to a stress of about 2.5 GPa. Both bands shift to lower frequencies with increasing stress, and at low stress there is very little distinction between their behaviors. The shift rate, calculated using results from four different samples at room temperature and the quoted filament diameter of 27 μm, is -5.5 ± 0.5 cm^{-1} GPa^{-1}. The large uncertainty is again attributed to the irregular cross section. As a consequence the values of stress in Figure 9 have been calculated to give agreement with the mean shift rate obtained at low stress, rather than simply assuming that this filament has a diameter of 27 μm.

At both temperatures the mean shift rate at low stress is found to be the same within experimental error. Differences observed with temperature relate to the increased shift rate, seen at higher stresses, and the relative proportions of the two component bands. At stresses above about 1.2 GPa, one band continues to shift to lower frequencies with an increased gradient while the other shifts back to slightly higher frequencies and becomes insensitive to stress. At low temperature the increased shift rate is ~ -8 cm^{-1} GPa^{-1} and the balance between the high and low load bearing populations ~75:25. At room temperature a smaller fraction of the material sees the high load (proportion ~30:70) and the shift rate of this fraction is considerably greater,

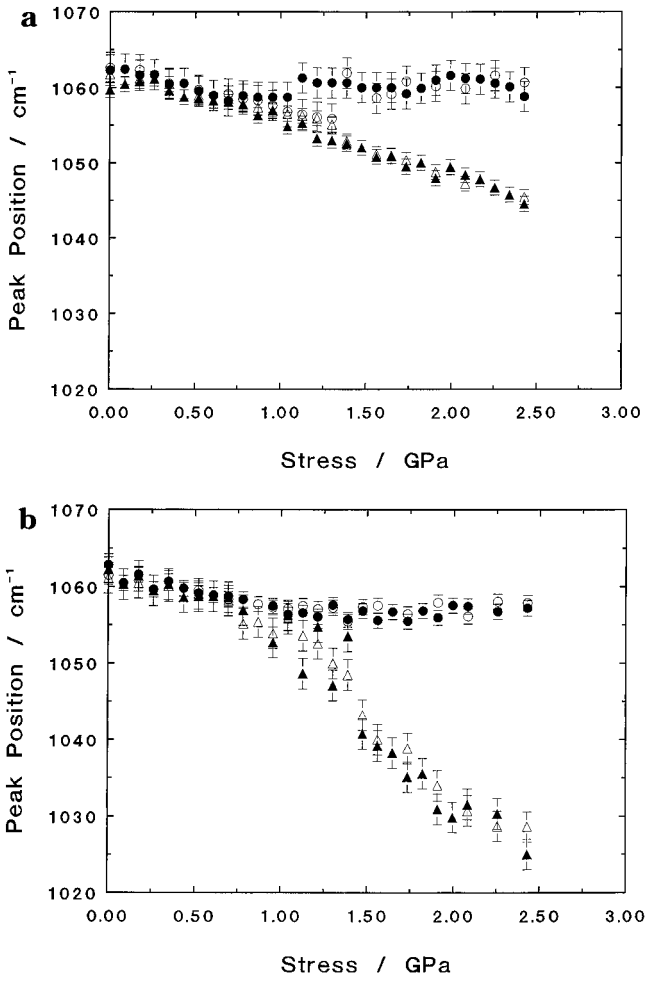

Figure 9. Variation in component band positions (of the C−C asymmetric stretching mode) as a function of stress at (a) −55 °C and (b) room temperature (+21 °C). High load bearing, ▲, and low load bearing, ●, components. Filled points correspond to the first and second runs on this sample and the open points to the third and fourth runs. The run order was −55 °C, 21 °C, −55 °C, and 21 °C.

~ -19 cm^{-1} GPa^{-1}. Generally, the features of inhomogeneous behavior evident in X-ray diffraction are also shown by the Raman technique.

Measurements obtained using the argon ion laser and an incident polarization parallel to the fiber axis yielded the same results, confirming that the technique is independent of both polarization and wavelength. In addition the limited investigations of the 1125 cm^{-1} band showed no difference in the basic behavior.

Discussion

Results from the three techniques presented above all derive from samples which have been subjected to the same stress history. The mechanical measurements directly measure the macroscopic strain while X-ray diffraction provides the crystalline strain. The Raman results are more difficult to interpret because there is some ambiguity concerning the regions to which they relate and the parameter they probe. These complications render it prudent to first interrelate the mechanical and X-ray scattering results, both of which are unambiguous, before attempting to interpret the Raman results. In essence this involves identification of a suitable structural model, since ultimately all results relate to this.

An insight into the structural nature of a material can be gained by examining the temperature dependence of the apparent crystal modulus, E_c^{app}, defined as the ratio of macroscopic stress to crystalline strain. (Note that for homogeneous stress transfer the crystalline stress is identical to the macroscopic stress and E_c^{app} is the true crystal modulus.) Britton et al.[22] and Clements et al.[23] have investigated this in melt spun and drawn polyethylenes of low and high draw ratios and have related differences in behavior to structural differences. At a low draw ratio the materials have a series lamellar structure, and relatively homogeneous stress transfer dominates. At higher draw ratios the structure resembles a continuous crystal containing amorphous regions. The greater temperature dependence of E_c^{app} is attributed to differing degrees of stress concentration around the crystallites as the modulus of the noncrystalline regions changes with temperature. It was concluded[23] that E_c^{app} approaches a value of about 255 GPa at low temperature, regardless of material or draw ratio and that this value sets a lower limit to the true crystal modulus.

The current work on gel-spun fiber shows that the crystalline response at low stress is basically the same at all three temperatures (i.e. E_c^{app} is independent of temperature). The simplest interpretation of these results is that the stress is homogeneously distributed through the system, in which case, the value of 290 GPa, found from the slope of this line, approximates the true crystal modulus. This agrees well with the theoretical prediction[24] of 315 GPa and a value of 329 GPa found in neutron scattering,[25] both of which relate to low temperature measurements, as well as with that reported for a single fiber of *Spectra*[7,19] at room temperature.

A simple series model can account for the apparent homogeneous stress distribution seen in the crystal strain experiment (temperature independent E_c^{app}) but fails to describe the observed macroscopic mechanical properties unless the noncrystalline content is very small (<5%). This implies a crystallinity in excess of 95%, conflicting with that measured here (80%) and the value of 75% reported elsewhere.[26] On the other hand, a parallel model is more successful in predicting macroscopic behavior, but since it also predicts a temperature dependent E_c^{app}, it is not suitable. These two models predict the upper and lower bounds to the macroscopic modulus for samples of specific crystallinity. Intermediate values for the macroscopic properties can be obtained using Takayanagi models,[13] which combine features of these two models. The specific predictions depend on the nature of the stress transfer, in the direction normal to the applied stress, between units in the model; since this is indeterminate in this case, these models are not considered here.

This problem of stress transfer between elements in a model is handled more successfully by short fiber composite models.[27] Cox[28] derived an expression for the case of an elastic fiber perfectly bonded in an elastic matrix with no load transfer occurring through the fiber ends. In its more common form, for hexagonal packing of the fibers, the model relates the macroscopic modulus, E, to the moduli and volume fractions V of the fiber and matrix components:

$$E = E_f V_f \Phi + E_m V_m \tag{1}$$

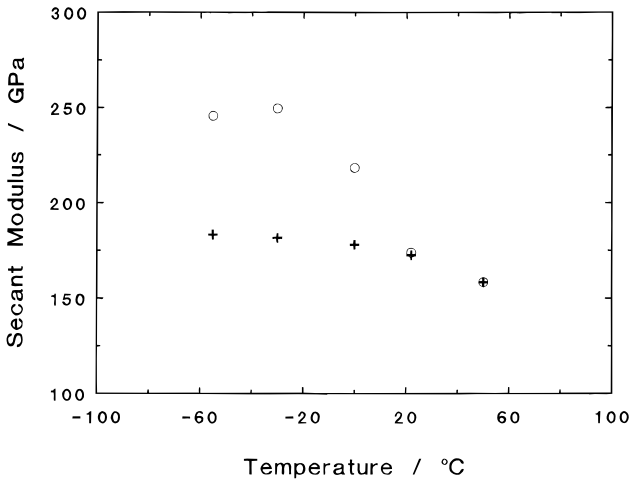

Figure 10. The predicted moduli (+) as a function of temperature for *Spectra* fiber using the Cox fiber composite model. The observed secant moduli (○) are shown for comparison.

where

$$\Phi = 1 - \frac{\tanh\left(\frac{\beta L}{2}\right)}{\frac{\beta L}{2}} \tag{2}$$

and

$$\frac{\beta L}{2} = 2A\left(\frac{G_m}{E_f \ln(\pi/2\sqrt{3}V_f)}\right)^{1/2} \tag{3}$$

G_m is the shear modulus of the matrix, and A is the aspect ratio of the fiber. The shear lag factor, Φ, can be regarded as a measure of the efficiency of reinforcement. The exact form for Φ varies with different fiber composite models, and the implications of this will be discussed later.

The model is applied here by identifying the fiber and matrix with the crystalline (80%) and amorphous phases, respectively. The modulus of the amorphous phase, E_a, is assumed to be given by

$$E_a = 3G \tag{4}$$

where G is the shear modulus, while the value for the aspect ratio, 30, is obtained by matching model predictions to the observed modulus at 50 °C. Measurements of the temperature dependence of the shear modulus of highly oriented polyethylene[29] are used to predict the temperature dependence of E_a and Φ, and thereby, the tensile modulus. The predicted and experimental values of the modulus are compared in Figure 10. The model clearly predicts the general change in modulus with temperature, but the observed modulus shows a significantly greater sensitivity than predicted. Indeed, according to the model, the value for the shear lag factor, Φ, increases from 0.66 at 50 °C to 0.76 at −55 °C. In contrast, the experimental measurements would require an increase from 0.66 to about 1 over the same temperature range. Moreover, the maximum attainable modulus, which according to the model occurs when $\Phi = 1$, is about 240 GPa (assuming values for E_a in eq 1 are low). This is equal to, or less than, some of the low temperature measurements, and the discrepancy is likely to become more significant at lower temperatures.

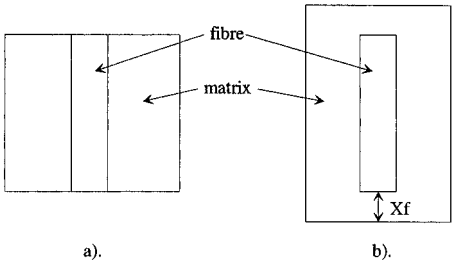

Figure 11. Elementary cell with (a), no matrix and (b), some matrix, X_f, present at the fiber ends.

It is also important to check the consistency between the model and the X-ray measurements. The essence of the fiber composite model is that stress in the fiber builds up along its length to a maximum at the center so that, consequently, the strain within the fiber is not constant. Therefore, for samples containing crystalline regions in the fibers, the model predicts a broad spectrum of crystalline strains, with the shape of the spectrum depending on how the stress builds up along the fiber length and the distribution of fiber lengths present in the material. Over the range of temperatures investigated, however, the X-ray measurements suggest that at low stress there is no strain inhomogeneity in the crystals. At high stress, on the other hand, there is strain inhomogeneity, but the distribution of crystalline strains can be modeled successfully by assuming two distinct populations, one of which shows very little strain. For fully crystalline fibers in a noncrystalline matrix, the relative proportion of the high strain (high load bearing) population can be taken as a measure of the fraction of the fiber providing effective reinforcement and corresponds to the parameter Φ in the model. In line with changes in Φ predicted above, the proportion of the high load-bearing crystalline fraction should fall from 76% to 66% as the temperature is increased from −55 to 50 °C. The X-ray measurements suggest that the fraction falls from about 75% to 20%. This change is clearly greater than that predicted by the model.

These problems, however, should not obscure the considerable advantage of this simple fiber composite model to explain strain inhomogeneity in the crystalline phase. The task is to reconcile the apparent homogeneous behavior at low stress with the greater than predicted strain inhomogeneity at high stress. Some of these problems are undoubtedly due to the simplicity of the model considered by Cox, in particular, the failure to consider stress transfer at the fiber ends and possible inelastic behavior of the matrix at high stresses. These aspects are discussed below.

More sophisticated treatment of the composite model has shown that the modulus depends significantly on three elements, the unit cell, the cell packing, and the stress transfer from the matrix to the fiber. Cox considered a basic unit cell with no matrix present at the fiber ends, (Figure 11a). It is, however, possible to construct a unit cell with a fraction, X_f, of the matrix present at the ends of the fiber while keeping the fiber volume fraction constant (Figure 11b). Berthelot et al.[30] showed that the modulus of a composite with this type of unit cell is dependent on the cell packing (Figure 12). Side-by-side regular packing with overlapping ends (Figure 12b) gives a significantly higher modulus than when the ends do not overlap (Figure 12a).

The value of 30 for the aspect ratio of the reinforcing unit is much greater than the crystalline aspect ratio of 1−3 obtained from X-ray diffraction[12] so the reinforcing element in the composite is unlikely to be the crystallite. A better candidate is the fibril which is a proven morphological feature of this material and has an aspect ratio of about 30.[12] These conclusions are in agreement with those of Prevorsek et al.,[15] who have also considered the composite as being composed of hexagonal cells (Figure 12b). The results presented here suggest that the most likely structure is a fiber composite, but a more sophisticated analysis, including consideration of the nature and packing of the elementary cells, needs to be taken into account if the magnitude of the changes are to be predicted correctly.

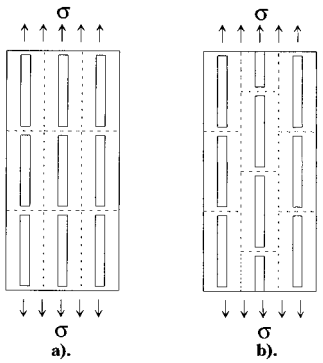

Figure 12. Packing of elementary cells: (a) side-by-side regular packing with non-overlapping fiber ends and (b) packing with overlapping ends.

As mentioned above, in addition to the cell packing the nature of the stress buildup along the fiber is also important. This is often discussed in terms of the critical length, l_c, which is twice the distance over which the fiber strain rises from zero to the maximum level. As the critical length, l_c, increases, a larger proportion of the fiber becomes less effective in its reinforcement, and the proportion which does provide the reinforcement will show a larger strain. Stress buildup along the fiber according to the Cox model assumes an elastic matrix. Other models, for example that of Kelly and Tyson,[31] consider the case of a plastic matrix and conclude that the stress buildup is not as sharp as this; in other words, l_c increases, and the reinforcement is less efficient. In practical studies, Galiotis et al.[3] have examined the behavior of a polydiacetylene single-crystal fiber in an epoxy resin matrix. In this case, the buildup of stress depended on two factors, the level of strain and the nature of the bonding. At low matrix strain, the stress and strain in the fiber were homogeneous, but at high matrix strain the stress buildup along the fiber followed the Cox model reasonably well. After repeated loading at very high stress, however, inelastic effects were observed and, simultaneously, the stress buildup at the fiber ends was found to be considerably less efficient; this process was attributed to debonding between the fiber and the matrix. In this way the load bearing length of the fiber was shortened and the effective critical length, l_c, increased. The current observations of homogeneous behavior at low stress and pronounced inhomogeneity at high stress in the crystalline component are very similar to the behavior of the polydiacetylene single-crystal fiber.

Clearly then, the nature of the stress buildup depends on several factors. Proper consideration of the tensile transfer of load to the matrix at the fiber ends, a consideration ignored by the Cox approach, can explain the more homogeneous stress and strain distribution at low strains. On the other hand the assumption that the matrix behaves elastically is probably invalid at

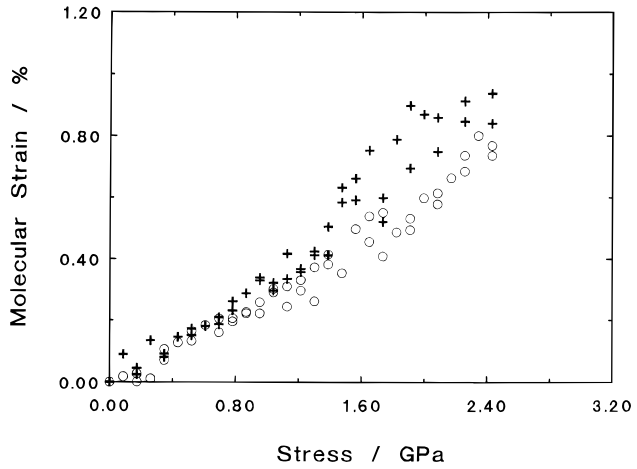

Figure 13. Average Raman strain as a function of stress at −55 °C (○) and 21 °C (+).

high stress. Indeed, Figure 6 provides good evidence for inelastic behavior at very high stress. Both the move to higher strain and the decrease in the proportion of the high load bearing population, seen at longer times, can be explained by an increase in l_c, which would be expected from a change to inelastic behavior.

It is now appropriate to consider the Raman results in the light of the conclusions derived from the comparison of X-ray and mechanical measurements. The 1060 cm^{-1} C−C asymmetric stretching band is generally accepted to arise from material in the stereoregular *trans*-conformation, a conformation adopted by both crystalline stem lengths and taut tie molecules. The vibrational frequency of this (and any) mode is determined by the local field in which the vibration occurs, so an applied strain which induces local conformational changes is likely to have a strong influence. In a multiphase system, however, the application of an external force will lead to a range of different values of stress and strain at the microscopic level. The relation between pure axial strain along the chain direction and vibrational frequency, therefore, may not be unique in such systems.

Wool et al.[2] derived a theoretical shift rate of −5.8 cm^{-1} GPa^{-1} for the 1060 cm^{-1} C−C asymmetric stretching band by using a Morse potential function to describe the anharmonic nature of the chemical bond. (i.e. the bond force constant decreases with increasing interatomic distance). If the polyethylene chain has a modulus E, the band shift rate, s, can be used to define a Raman strain, e, given by

$$e = \frac{\Delta\nu}{sE} \tag{5}$$

where $\Delta\nu$ is the change in the Raman frequency due to the application of stress. E is assumed to be 290 GPa, consistent with the findings on crystal strain measurements. Rather than considering the strains in the different populations, it is more convenient and more accurate to consider the average Raman strain. Figure 13 illustrates how the average Raman strain, derived from this equation, varies with macroscopic stress at −55 °C and room temperature. In the low stress region at both temperatures the response is practically the same within experimental error. At high stress the average Raman strain continues on the same curve to a first approximation, suggesting that stress distribution between the different phases is not changing.

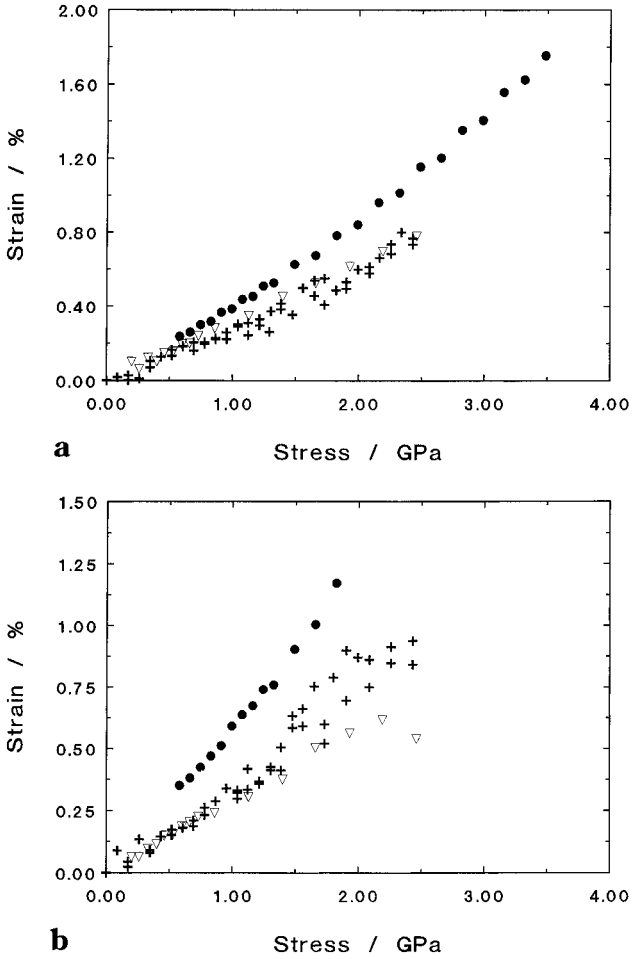

Figure 14. Comparison of macroscopic strain (●), average crystal strain (▽), and average Raman strain (+) as a function of macroscopic stress at (a) −55 °C and (b) room temperature (21 °C).

However, closer investigation shows that the response of the average Raman strain in this region is temperature dependent with a larger Raman strain being produced at high temperature, indicating that the Raman sensitive component is taking a larger share of the strain. This contrasts with the X-ray results, which show an apparent strain saturation and probably arises because of the presence of taut tie molecules, which are included in the Raman measurements.

The three measures of strain are compared as a function of stress at −55 °C and 21 °C in parts a and b of Figure 14, respectively. Since all are measured in response to the same stress history, it is possible to check whether Raman and X-ray measurements are directly equivalent. At both temperatures the macroscopic strain is significantly greater than the crystal strain. At low stresses, the responses of Raman strain and crystal strain are very similar at both −55 °C and room temperature. At room temperature, however, there is a significant discrepancy between Raman strain and crystal strain in the high stress region. This probably arises because the Raman technique is sensitive not only to the crystalline species, but also to taut tie molecules.

This is shown more clearly in parts a and b of Figure 15 where the behaviors of the two load-bearing components, as monitored using the Raman and X-ray techniques, are considered. At both temperatures the Raman strain and crystal strain are equivalent when the applied stress is low. The situation is different at

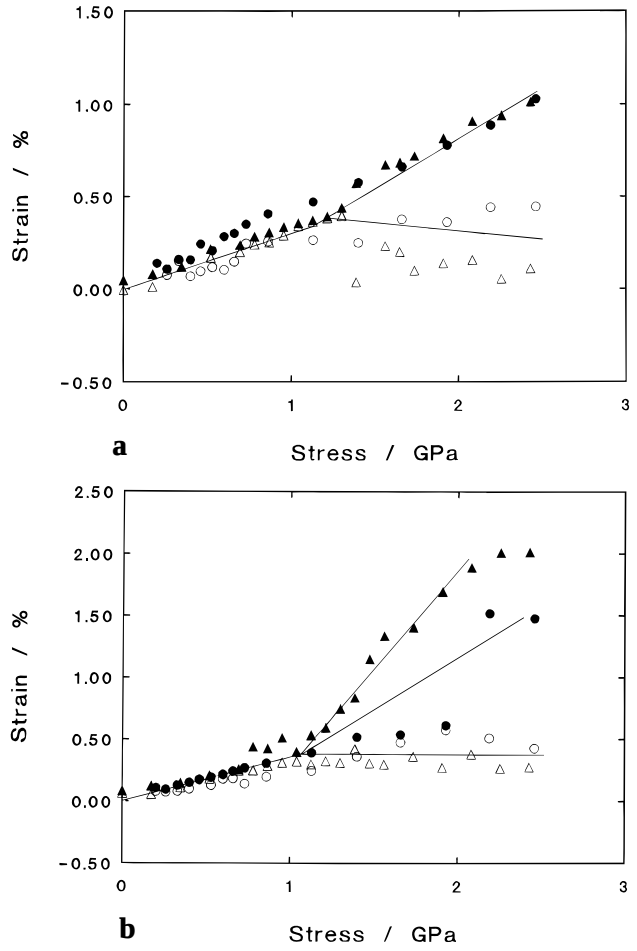

Figure 15. Separate high and low load-bearing component contributions to crystal strain (●) and Raman strain (▲) as a function of macroscopic stress at (a) −55 °C and (b) room temperature (21 °C). Filled and open points correspond to high and low load-bearing components, respectively.

high stress. First, at low temperature, the two techniques show similar trends for the high load-bearing component, whereas the low load-bearing component shows a slightly higher level of strain in the X-ray than in the Raman. The analysis adopted here assumes that there are two discrete populations rather than, as might be expected with a fiber composite, a spectrum of stresses. In addition, the data obtained in X-ray diffraction relate to a multifilament bundle where, despite the careful mounting, there is likely to be a natural spread in the individual filament stress. This spread may well explain the fact that the separation in behaviors of the two components at a particular stress is more clearly seen in the Raman, but overall the agreement is very good.

At high temperature, an additional discrepancy is introduced, with the high load bearing component showing a greater strain in the Raman than in the X-ray. This may relate to an additional contribution from taut tie molecules, specifically those in parallel with the fiber ends which might be expected to show a significant strain to counterbalance the inefficient transfer of stress to the fiber ends. Nevertheless the considerable agreement between both techniques, including the correspondence in the position of the peak splitting and the relative distribution of stress between the two populations, basically suggests that the Raman technique is effectively monitoring the crystal strain.

Conclusions

X-ray measurements of the crystal strain at different temperatures suggest that at low strains there is effectively homogeneous stress throughout the sample, although the slight asymmetry of the (002) profile shows that there is a small deviation from this. A value of 290 GPa was found for the lower limit to the crystal modulus. This value replaces the earlier value of 255 GPa found in this laboratory and is considered to be a more reliable estimate of the actual crystal modulus because of the lack of a dependence on temperature. It is also in better agreement with both theoretical and other experimental values.

The X-ray and macroscopic strain measurements are best explained by a fiber composite model in which attention has to be paid to the packing of the reinforcing elements. The fiber composite model has the advantage that it can describe qualitatively the asymmetry in the (002) diffraction peak. Furthermore the pronounced asymmetry and time dependent behavior of the X-ray measurements at high strain may arise because the matrix behaves nonelastically at these high stresses.

Values of strain obtained from the Raman spectra depend critically on the assumptions involved in the analysis but generally lie very close to values obtained from the X-ray measurements if accepted values for the intrinsic band shift rate are used. In addition, general features, such as the small temperature dependence of the band shift rate and the observations at high strain are very similar to observations made using X-ray diffraction. At room temperature, however, there is a clear distinction between the Raman and X-ray techniques at high stress, probably arising from the fact that the Raman measurements relate to both trans sequences in the crystalline regions and taut tie molecules.

Acknowledgment. T.A. gratefully acknowledges the support of the Thai Government. A.P.U. was supported by a grant from the EPSRC. We wish to thank Dr. C. Cheng and Mr. K. Baldwin with regard to obtaining and analyzing the Raman spectra.

References and Notes

(1) Sakurada, I.; Nukushina, Y.; Ito, T. *J. Polym. Sci.* **1962**, *57*, 651.
(2) Wool, R. P.; Bretzlaff, R. S.; Li, B. Y.; Wang, C. H.; Boyd, R. H. *J. Polym. Sci., Polym. Phys. Ed.* **1986**, *24*, 1039.
(3) Galiotis, C.; Young, R. J.; Yeung, P. H. J.; Batchelder, D. N. *J. Mater. Sci.* **1984**, *19*, 3640.
(4) Robinson, I. M.; Yeung, P. H. J.; Galiotis, C.; Young, R. J.; Batchelder, D. N. *J. Mater. Sci.* **1986**, *21*, 3440.
(5) Lewis, E. L. V.; Bower, D. I.; Ward, I. M. *Polymer* **1995**, *36*, 4741.
(6) Tashiro, K.; Wu, G.; Kobayashi, M. *Polymer* **1988**, *29*, 1768.
(7) Prasad, K.; Grubb, D. T. *J. Polym. Sci., Polym. Phys. Ed.* **1989**, *27*, 381.
(8) van Eijk, M. C. P.; Leblans, P. J. R.; Meier, R. J.; Kip, B. J. *J. Mater. Sci. Lett.* **1990**, *9*, 1263.
(9) Kip, B. J.; van Eijk, M. C. P.; Meier, R. J. *J. Polym. Sci., Polym. Phys. Ed.* **1991**, *29*, 99.
(10) Wong, W. F.; & Young, R. J. *J. Mater. Sci.* **1994**, *29*, 510.
(11) Moonen, J. A. H. M.; Roovers, W. A. C.; Meier, R. J.; Kip, B. J. *J. Polym. Sci., Polym. Phys. Ed.* **1992**, *30*, 361.
(12) Grubb, D. T.; Prasad, K. *Macromolecules* **1992**, *25*, 4575.
(13) Takayanagi, M.; Imada, K.; Kajima, T. *J. Polym. Sci.* **1966**, *C15*, 263.
(14) Wong, W. F.; Young, R. J. *J. Mater. Sci.* **1994**, *29*, 520.
(15) Prevorsek, D. C.; Chin, H. B.; Murthy, S. *J. Polym. Sci., Polym. Symp.* **1993**, *75*, 81.
(16) Lovell, D. R. *Carbon and high performance fibres directory*, 5th ed.; Chapman & Hall: London, 1991.
(17) Gupta, V. B.; Ward, I. M. *J. Macromol. Sci., Phys.* **1967**, *B1*, 373.

(18) Troughton M. J.; Davies, G. R.; Ward, I. M. *Polymer* **1988**, *29*, 1389.
(19) Prasad, K.; Grubb, D. T. *J. Polym. Sci., Polym. Phys. Ed.* **1990**, *28*, 2199.
(20) Mitra, V. K.; Risen, W. M, Jr.; Baughman, R. H. *J. Chem. Phys.* **1977**, *66*, 2731.
(21) Batchelder, D. N.; Bloor, D. *J. Polym. Sci., Polym. Phys. Ed.* **1979**, *17*, 569.
(22) Britton, R. N.; Jakeways, R.; Ward, I. M. *J. Mater. Sci.* **1976**, *11*, 2057.
(23) Clements, J.; Jakeways, R.; Ward, I. M. *Polymer* **1978**, *19*, 639.
(24) Tashiro, K.; Kobayashi, M.; Tadokoro, H. *Macromolecules* **1979**, *11*, 914.
(25) Feldkamp, L. A.; Venkataraman, G.; King, J. S. *Neutron inelastic scattering*; Vol. 2, Proceedings of the Symposium, Copenhagen, 1968, IAEA: Vienna, 1968; p 159.
(26) Prevorsek, D. C.; Chin, H. B.; Kwon, Y. D.; Field, J. E. *J. Appl. Polym. Sci., Appl. Polym. Symp.* **1991**, *47*, 45.
(27) Holister, G. S.; Thomas, C. *Fibre Reinforced Materials*; Elsevier Publishing: London, 1966; pp 14−66.
(28) Cox, H. *Br. J. Appl. Phys.* **1952**, *3*, 72.
(29) Maxwell, A. S. Ph.D. Thesis, University of Leeds, 1994.
(30) Berthelot, J.-M.; Cupcic, A.; Brou, K. A. *J. Compos. Mater.* **1993**, *27*, 1391.
(31) Kelly, A.; Tyson, W. R. *J. Mech. Phys. Solids* **1965**, *13*, 329.

MA961462T